Opto-Electronic Advances

Review

2018, Vol. 1, No. 3

DOI: 10.29026/oea.2018.180005

850/940-nm VCSEL for optical communication and 3D sensing

Chih-Hsien Cheng[1†], Chih-Chiang Shen[2†], Hsuan-Yun Kao[1], Dan-Hua Hsieh[2], Huai-Yung Wang[1], Yen-Wei Yeh[2], Yun-Ting Lu[2], Sung-Wen Huang Chen[2], Cheng-Ting Tsai[1], Yu-Chieh Chi[1], Tsung Sheng Kao[2], Chao-Hsin Wu[1,3*], Hao-Chung Kuo[2*], Po-Tsung Lee[2] and Gong-Ru Lin[1,3*]

This paper is going to review the state-of-the-art of the high-speed 850/940-nm vertical cavity surface emitting laser (VCSEL), discussing the structural design, mode control and the related data transmission performance. InGaAs/AlGaAs multiple quantum well (MQW) was used to increase the differential gain and photon density in VCSEL. The multiple oxide layers and oxide-confined aperture were well designed in VCSEL to decrease the parasitic capacitance and generate single mode (SM) VCSEL. The maximal modulation bandwidth of 30 GHz was achieved with well-designed VCSEL structure. At the end of the paper, other applications of the near-infrared VCSELs are discussed.

Keywords: vertical cavity surface emitting laser; 3D sensing; optical communication; LiDAR; virtual reality; augmented reality

Cheng C H, Shen C C, Kao H Y, Hsieh D H, Wang H Y *et al*. 850/940-nm VCSEL for optical communication and 3D sensing. *Opto-Electronic Advances* **1**, 180005 (2018).

Background

To meet the demand on the rapid development of the internet at present, versatile laser diodes based optical fiber transmission has been widely applied not only in long-haul backbone (with single-mode fiber, SMF and distributed feedback laser diode, DFBLD) and medium-range metropolitan area networks (with SMF/DFBLD or single-mode vertical cavity surface emitting laser, VCSEL), but also in short-distance area networks or intra/inter data center links (with SMF/DFBLD or multi-mode fiber and multi-mode VCSEL). In recent years, the convergence and streaming with combinations of the broadband voice and video data urge the internet related industry to develop the advanced optical communication solutions which fulfill the huge global market need. All developed and developing countries have established the high-speed optical fiber network infrastructures to achieve both the fiber to the home (FTTH), cloud/mobile data storage and streaming, and the intra/inter data center applications, etc., which is an interdisciplinary integration and construction between wired and wireless communication services. Particularly, owing to the urgent requirement on the higher data transmission rate for the faster up-/down-stream data exchange in intra data centers, the currently available transmission link based on multi-mode VCSEL and multi-mode fiber at 10 Gbps/channel has gradually found its bottleneck to supply the tremendous network flux instantaneously. Beyond the specification of the 40/100 Gbps data center that has been commercially available, the definition and design of next-generation 400-Gbps or even 1.6-Tbps transceiver module based on high-speed VCSELs at 850 nm has also been initiated toward practical applications no later than 2020.

To catch up the developing pace of huge-amount data streaming in data center for the fusion among wireless mobile, wired telecom, cloud data center, and the FTTH networks in the near future, the investigation on the VCSEL based optical transceiver circuit module with optimized transmission data rate and extended propagation distance in multi-mode fiber become important key

[1]Graduate Institute of Photonics and Optoelectronics, Department of Electrical Engineering, Taiwan University, Taipei 10617, China; [2]Department of Photonics & Graduate Institute of Electro-Optical Engineering, College of Electrical and Computer Engineering, Chiao Tung University, Hsinchu 30100, China; [3]Department of Electrical Engineering, Taiwan University, Taipei 10617, China.

[†]These authors contributed equally to this work.

* Correspondence: G R Lin, E-mail: grlin@ntu.edu.tw; H C Kuo, E-mail: hckuo@faculty.nctu.edu.tw; C H Wu, E-mail: chaohsinwu@ntu.edu.tw

Received 16 March 2018; accepted 25 April 2018; accepted article preview online 27 April 2018

technologies. Especially for the required transmission capacity of the cloud transmission within intra- or among inter-data-center networks, more than millions of VCSEL-multi-mode fiber (MMF) links for cloud computing located within super data centers with the least space beyond 100,000 ft^2 and the consumed power above 10 MW, which inevitably lengthens the distance between the server rooms and even among the different severs in the sever room to make the transmission line more complicated. Therefore, each VCSEL based transceiver module has to enhance its transmission rate to 100~400 Gbps to improve the total data transmission capacity in a distance as short as 50~100 m such that the module size, energy consumption and maintaining cost can be concurrently scaled down. Moreover, the fourth-generation intelligent mobile communications (4G) with the wireless transmission rate from 5 to 208 Mbps can transmit the telephone, e-mail and video and other multimedia information. For the fifth-generation intelligent mobile communications (5G), the wireless transmission rate may be achieved to 10 Gbps, which is 100 times larger than that of 4G communication. Therefore, the large capacity and fast transceiver rate of 400 Gbps optical communication provides a key technology to apply to Internet of Things (IoT), mobile networking, super high definition video, and big data. To achieve the requirement of the high-speed and large-capacity to apply to the super computers, cloud computing, and data centers, the VCSEL is developed to become the light source of the short-reach optical links because this laser has some advantages including the low power-consumption, the effectively coupling to fiber, the low threshold current, and the high power conversion efficiency.

Design of the high-speed 850-nm VCSEL

To achieve the high-speed VCSELs, the carriers and photons directly influence the modulation speed of the VCSEL for data transmission. In principle, the relaxation frequency is the natural oscillation frequency between carriers and photons in the VCSEL which can be expressed as below:

$$2\pi f_r \cong \left[\frac{v_g a N_p}{\tau_p}\right]^{\frac{1}{2}} = \left[\frac{v_g a \Gamma \eta_i}{q V_p}(I - I_{th})\right]^{\frac{1}{2}}, \qquad (1)$$

where v_g is the group velocity, τ_p is the photon lifetime, I is the bias current, and I_{th} is the threshold current. In general, the relaxation resonance frequency of the intrinsic laser determines the device modulation speed. From Equation (1), the enhancement of the differential gain and photon density in VCSEL can effectively improve the modulation bandwidth. In 2009, Westbergh et al. changed the GaAs quantum well (QW) to the InGaAs QW to enhance the differential gain in the VCSEL. When using the InGaAs QW as the active layer, the 3-dB bandwidth of the VCSEL can be achieved to 20 GHz at 25 ℃ and 15.2 GHz at 85 ℃[1]. Healy et al. used the $In_{0.1}GaAs$ QW with the 6-pair quantum layers as the active layer to demonstrate the VCSEL with the 3-dB bandwidth of 19.5 GHz[2]. Figure 1 shows the simulated frequency responses of the VSCSEL under different photon densities. When increasing the photon density, the 3-dB bandwidth frequency of VCSEL can be enlarged. In 1996, Lear et al. increased the bias current to enlarge the photon density[3]. When increasing the bias current to 4.5 mA, the 3-dB bandwidth of the VCSEL was improved to 16.3 GHz[3]. Later on, they demonstrated the oxide-confined VCSEL with the maximal modulation bandwidth of 21.5 GHz at the bias current of 4.8 mA[4].

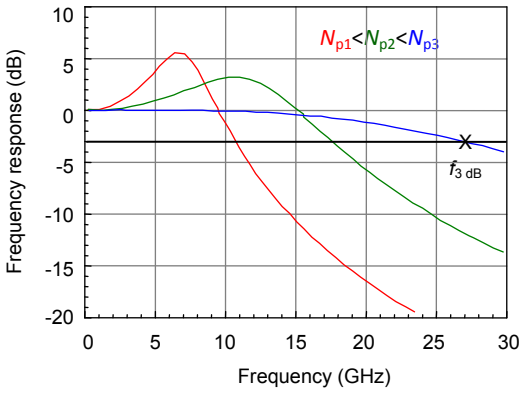

Fig. 1 | Schematic plot of intrinsic modulation response with increasing photon densities.

In addition, the second limitation on the modulation bandwidth of the VCSEL is originated from the parasitic resistance and capacitance. Figure 2(a) shows the parasitic capacitance and resistance elements existed in the VCSEL, where C_p is the pad capacitance, C_a is the active region capacitance and C_o is the oxide capacitance. These parasitic resistance and capacitance can be regarded as the low-pass filter to suppress the high-frequency response of the VCSEL, as shown in Fig. 2(b). The resistance inside the VCSEL is contributed by the DBR mirror resistance (R_m), and the active region resistance (R_a) including the current path confined by oxide aperture.

To decrease the parasitic capacitance, the multiple oxide layer was proposed to replace the single oxide layer because the device capacitance is inversely proportional to the oxide layer thickness[5-7]. Figure 3 shows the simulated frequency responses of the VCSEL with the single- and double-confined oxide layers. When employing the double-confined oxide layer, the parasitic capacitance of the VCSEL is effectively reduced to improve the device 3-dB bandwidth from 17.1 GHz to 21.1 GHz. The TEM image of the VCSEL with the double-confined oxide layer is shown in Fig. 4. Chang et al. utilized the tapered oxide layer to decrease the parasitic capacitance, which improves the modulation bandwidth to 13.2 GHz[5]. Ou et al. reported that the added thin oxide layer decreases the mesa capacitance without the increase of series resistance,

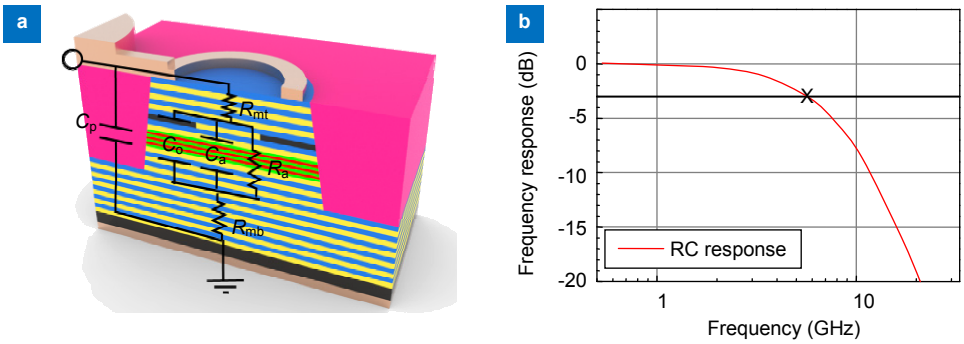

Fig. 2 | (**a**) Electrical parasitic elements inside a VCSEL. (**b**) Low pass filter induced by the RC components.

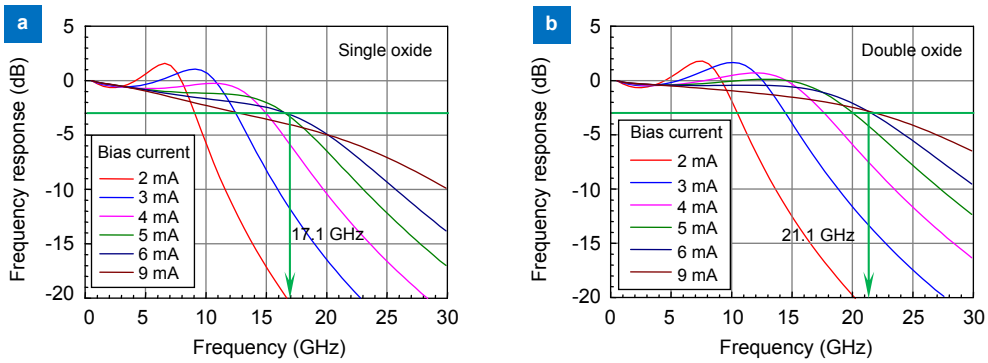

Fig. 3 | Simulated frequency responses of the 850-nm VCSEL with (a) single- and (b) double-confined oxide layers.

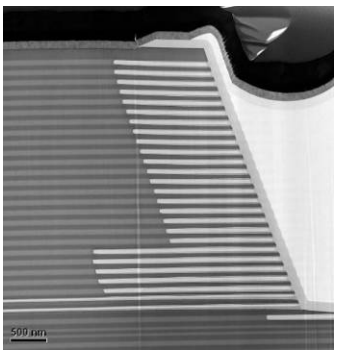

Fig. 4 | TEM image of the VCSEL with double-confined oxide layers.

which can enhance the 3-dB parasitic frequency to 30 GHz[6]. More recently, Feng's group used five InGaAs quantum wells and multiple confined oxide layer design to enhance the frequency response of the VCSEL because the multiple oxide can effectively decrease the capacitance of the device to further reduce the RC constant[7]. Without post-fabrication to detune the photon lifetime, the 3-dB modulation bandwidth is effectively enhanced to 28.2 GHz[7]. Moreover, some research reported that the thicker low-dielectric material like benzocyclobutene (BCB) was proposed to improve the parasitic capacitance of the VCSELs because this low-dielectric material has the lower capacitance[8,9]. This method is also called as the oxide relief to reduce the dielectric constant close to the air by etching away the oxide aperture[8,9]. In 2005, Tanigawa et al. used the BCB-planarized layer to replace the conventional silicon nitride passivation layer, which significantly reduced the 70% parasitic capacitance of the VCSEL[8]. This improvement makes the VCSEL with the relaxation oscillation frequency of 12 GHz operate at 70 ℃ over 750 hours[8]. In 2013, Shi et al. used this oxide-relief technology and Zn-diffusion to enhance the 3-dB bandwidth of the single-mode VCSEL to 12 GHz as compared to the conventional device[9].

The third limitation to restrict the modulation bandwidth of the 850-nm VCSEL is dominated by the internal heating induced thermal effect in the active layer of the device. Without considering the damping and electrical parasitic effects, the thermal effect induced maximal modulation bandwidth can be estimated as below[10]:

$$f_{3\,\mathrm{dB,max}} \approx \sqrt{1+\sqrt{2}}\, f_{\mathrm{r,max}} \quad , \tag{2}$$

where $f_{3\,\mathrm{dB,\,max}}$ and $f_{\mathrm{r,\,max}}$ denote the maximal 3-dB modulation frequency and relation oscillation frequency, respectively. AL-Omari et al. used the self-aligned top contact and evaporated gold or plated copper heatsink to reduce the thermal resistance to 44%, which can improve the 3-dB modulation bandwidth to 16.3 GHz by 12% increment[11]. In 2010, Larsson et al. used the InGaAs to replace the GaAs material, which can decrease the thermal impedance[12]. This decreased thermal impedance can improve the 3-dB modulation bandwidth of the VCSEL to 29 GHz[12].

Mode control of the high-speed 850-nm VCSEL

In the recent researches, the 850-nm multi-mode (MM) VCSELs combining with the MM fiber (MMF) to form the transmission link is one of the cost-effective solutions [13-15]. In 2009, Gholami et al. employed the modal dispersion in the MM fiber to compensate the chromatic dispersion, which further demonstrates 10 Gbps Ethernet systems by using the MM VCSEL and MM fiber transmission link[13]. In addition, Blokhin et al. used the MM VCSEL with the oxide-confined aperture to demonstrate the 39 Gbps non-return-to-zero (NRZ) data transmission under the error-free condition [14]. In 2010, Westbergh et al. used the same structure to improve the data rate to 40 Gbps under the back-to-back (BtB) transmission[15]. When transmitting 100-m MM fiber, the bit rate of the NRZ data can be achieved to 35 Gbps under the error-free condition[15]. However, the modulation bandwidth of the MM VCSEL limits the permissible data rate and transmission distance[16]. In 2012, Szczerba et al. reported the variation on the 3-dB bandwidth of the transmission system under different distances by using the MM VCSEL[16]. When the transmission distance increases to 800 m, the 3-dB bandwidth of the transmission system is suppressed from 8.5 GHz to 2.3 GHz[16]. In addition, the modal dispersion of transverse modes in MMF contributes to the crosstalk effect, which further degrades the data rate.

The reduction on the transverse modes of the MM VCSELs to improve the data transmission becomes an important issue[17-19]. In 2000, Choquette et al. increased the fundamental-mode gain by using the gain aperture, which increases the fundamental-mode selection to make the transverse mode of the VCSEL be improved to the single mode[17]. In 2004, Haglund et al. reported that the shallow surface relief within the 850-nm VCSEL can increase the high-order mode loss, which decreases the transverse modes of the device to single mode (SM)[18]. In 2005, Furukawa et al. employed the triangular hole to enhance the optical confinement in the VCSEL, which demonstrates the SM VCSEL[19]. In 2013, Safaisini et al. used the 3-mm oxide aperture to confine the transverse mode of the 850-nm VCSEL to quasi-single mode with the side-mode suppression ratio of 18 dB[20]. In general, shrinking the diameter of the oxide-confined aperture can enlarge the mode spacing to reduce the high-order mode generation, which further decreases the mode number of VCSEL[21] because the oxide-confined aperture provides transverse confinement for electrical current and optical fields. Figure 5 shows the optical spectra of VCSELs with different sizes of oxide-confined aperture under the bias condition of I=1.3 $I_{\rm th}$. The VCSEL with a smaller oxide aperture has the fewer existed optical mode due to the small lateral confinement aperture design. Larger oxide aperture induces the weak optical confinement, which further generates the more modes existed in the VCSEL.

In addition, the lateral modal distribution for VCSEL with different sizes of the oxide-confined aperture under various bias currents is shown in Fig. 6. The VCSEL with the smaller oxide-confined aperture has a clear optical mode distribution due to the existence of the fewer modes as compared to the device with the larger oxide-confined aperture. Moreover, the VCSEL with the larger oxide-confined aperture has a more non-uniform modal distribution due to non-uniform current injection at a high bias current. The decrease of carrier density in the center region of the aperture is occurred due to spatial hole burning (SHB) effect[22-24]. As a result, the VCSELs with the large oxide-confined aperture favors high order modes in the peripheral region at a high bias current and non-uniformity of transvers modes can be observed as shown in Fig. 6(b). Figure 6(c) shows the cross-sectional SEM picture of VCSEL.

In addition, the small-size oxide-confined aperture increases the current density, which contributes to the improvement of the 3-dB modulation bandwidth ($f_{3\,\rm dB}$). Figure 7 shows the frequency response of the VCSEL with different-size oxide-confined apertures. The maximal 3-dB bandwidth of the VCSEL with the oxide-confined apertures of 6 μm and 10 μm is 17.5 GHz at 12 mA and 15.9 GHz at 13 mA, respectively.

However, the oxide confinement method increases the differential resistance of the device, which needs the same current injection carriers under the higher bias, which also induces the impendence mismatch to degrade the data transmission[25]. Therefore, the high-doping zinc-diffusion technology was used to improve the resistance of p-type layer for VCSELs, which further decreases the free-carrier absorption to enhance the quantum efficiency of the VCSEL[26,27]. On the other hand, the Zn-diffusion into the VCSEL device can create the selective loss of the high-order transverse modes to easily generate the SM VCSEL. In 1992, Yang et al. used the helium implantation and Zn-diffusion technology to demonstrate SM VCSEL with the linewidth of 0.4 nm[27]. In addition, Shi et al. reported the SM VCSEL with the 3-dB bandwidth of 12 GHz by using the Zn-diffusion technology[28]. In 2017, Kao et al. studied different transverse mode based Zn-diffused VCSEL by using the different oxide-confined apertures[29]. When decreasing the oxide-confined aperture, the transverse mode of the 850-nm VCSEL can be transferred from multi mode to single mode, as shown in Fig. 8[29]. In addition, the 3-dB modulation bandwidth of the device can be improved from 12 GHz to 23.5 GHz[29].

In principle, the future research directions to improve the bandwidth of the VCSEL will include the adjustment on RC time constant of the VCSEL by decreasing either its capacitance or resistance. One straightforward way is to decrease the mesa area of the VCSEL, which can effectively reduce the device capacitance. However, this

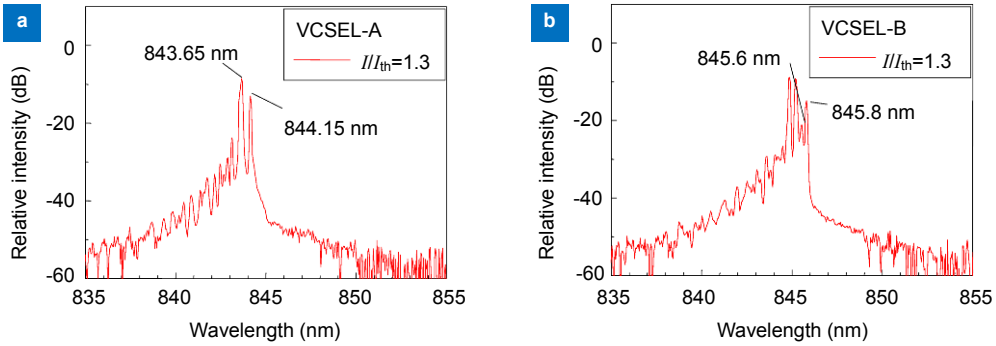

Fig. 5 | Optical spectra of the VSCELs with (a) 6-μm and (b) 10-μm oxide confined apertures.

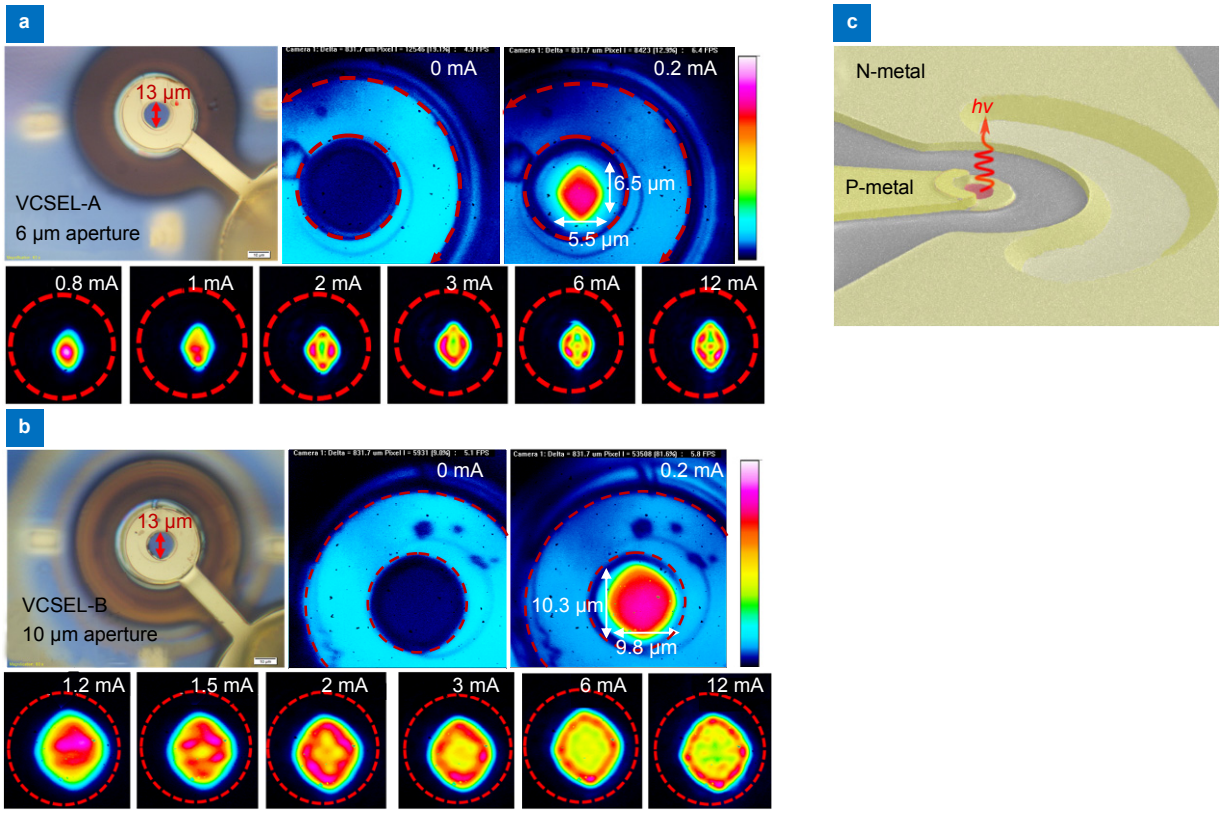

Fig. 6 | Near field lateral modal distributions of the VSCELs with (a) 6-μm and (b) 10-μm oxide confined apertures under different bias current conditions and (c) Cross-sectional SEM image of the VCSEL.

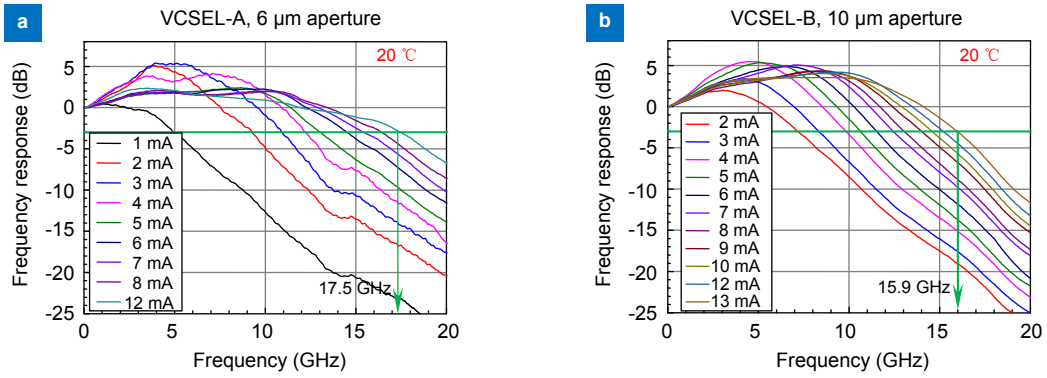

Fig. 7 | Frequency responses of the VSCELs with (a) 6-μm and (b) 10-μm oxide confined apertures under different bias current conditions.

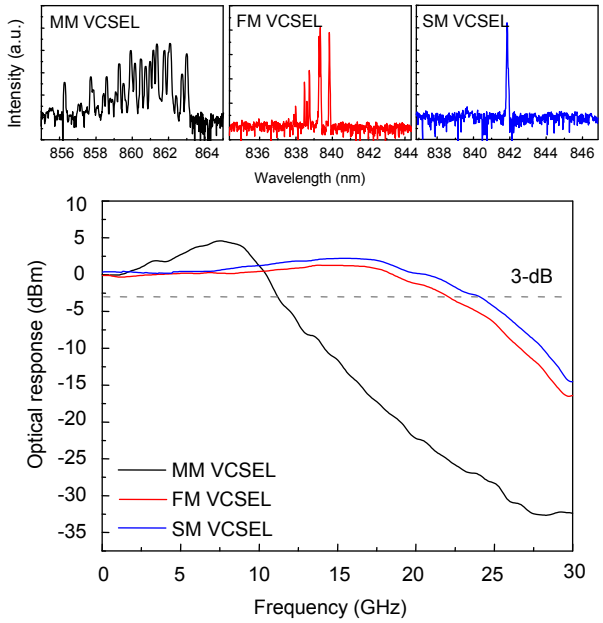

Fig. 8 | Optical spectra and frequency responses of the different-type VCSELs.

method would concurrently increase the device resistance. Therefore, the increasing doping density is expected to solve the increment on device resistance caused by reducing mesa area. The enhancement of device bandwidth is expectable with aforementioned processes. In addition, another potential approach relies on improving the epitaxial quality during growth, which effectively reduces the defects in the VCSEL so as to decrease the device resistance.

Data transmission performance of the high-speed VCSEL

For practical applications, several studies of the VCSEL for intra-data center links have been reported. In 2013, Westbergh et al. used the VCSEL with the 7-μm oxide-confined aperture to achieve the maximal modulation depth to 27 GHz, which performs the NRZ-OOK data transmission at 44 Gbps over 50-m OM4 fiber and at 47 Gbps under BtB condition[30]. In addition, the same group detuned the oxide-confined aperture diameter than before to improve modulation efficiency and impedance matching[31]. The maximal data rate can be enhanced to 55 Gbps at BtB condition and 43 Gbps over 100-m OM4 fiber[31]. In 2016, Shi et al. further employed the Zn-diffusion technology and oxide-relief aperture to obtain the quasi-SM VCSEL with the modulation bandwidth of 27 GHz, which processed the 54 Gbps NRZ-OOK data transmission with the bit error rate (BER) of 1.4×10^{-4} over 1-km OM4 fiber[32]. Feng's group further utilized the as-grown epitaxial structure of the 850-nm VCSEL without the post-fabrication to detune the photon lifetime, which acquired the 3-dB bandwidth of the device to 28.2 GHz[7]. Under BtB transmission, the 50 Gbps NRZ data transmission can obtain the BER of 10^{-12} at the receiving power of 0.5 dBm[7].

For the NRZ-OOK data transmission, the data rate is mostly dependent on the modulation bandwidth of the VCSEL because of the lower spectral usage efficiency for the NRZ-OOK data transmission. To solve this problem, the versatile data formats have been developed. The 4-level pulse amplitude modulation (PAM-4) data format is one of solutions to approach for decoding the VCSEL because the half of modulation bandwidth for the PAM-4 data format is used to achieve the same data rate as compared to the NRZ-OOK data format[33,34]. In 2011, Ingham et al. employed the oxide-confined VCSEL with the modulation bandwidth of 20 GHz to demonstrate the 32 Gbps PAM-4 data transmission with the BER below the forward error correction (FEC) criterion of 3.8×10^{-3} by using the pre-distortion technology[35]. In 2015, Szczerba et al. used the directly modulated 850-nm VCSEL carrying with the PAM-4 data format to achieve 60 Gbps over 2-m MMF and 50 Gbps over 50-m MMF[36]. In 2016, Castro et al. employed a pre-distortion technology to improve the data performance, which further demonstrates the 50-Gbit/s PAM-4 transmission over 200-m wideband multi-mode fibers (WBMMFs)[37]. In addition, Finisar Corporation demonstrated 4 channel 45 Gbps VCSEL chip over 300-m OM4 fiber by using the PAM-4 data format[38]. The BER of VCSEL chip is achieved below the KP4 criterion of 2×10^{-4}, which further obtains the total data rate to 180 Gbps[38]. In 2017, Kao et al. changed the mode number of the VCSEL to observe the transmission performance of the PAM-4 data format for the VCSEL with different transverse modes[29]. The MM VCSEL chip with the widest spectral linewidth and the highest optical power provides the smallest modulation bandwidth to obtain only 44 Gbps data under BtB transmission[29]. When decreasing the mode numbers to the few mode (FM), the data rate of the FM VCSELs is effectively enhanced to 52 Gbps. However, the data of the SM VCSEL is slightly degraded to 50 Gbps because of its higher differential resistance and lower power saturation to suppress the transmission capacity even though SM VCSEL has the largest modulation bandwidth[29]. After 100-m MM fiber transmission, the modal dispersion degraded the data rates from 34 Gbps to 28 Gbps as the transverse mode of the VCSEL transfers from multi mode and single mode.

Moreover, a pre-emphasis filter technology for the PAM-4 data format was proposed to apply to VCSEL, which further improves the data rate to 100 Gbps over 100-m MM fiber[39]. In 2018, the same group employed the pre-emphasizing technology to demonstrate the SM VCSEL based PAM-4 data transmission above 50 Gbps over 100-300-M OM4 fiber[40]. With the modulation bandwidth of the SM VCSEL at 18.9 GHz, the data rate of PAM-4 data can be achieved to 64 Gbps under BtB

transmission and over 100-m MMF, as shown in Fig. 9. When increasing the MMF distance from 200 to 300 m, the low-to-high frequency spectral power transformation is induced to suppress the peak-to-peak signal amplitude of the PAM-4 data, which further decreases the transmission capacity to 48 Gbps[40].

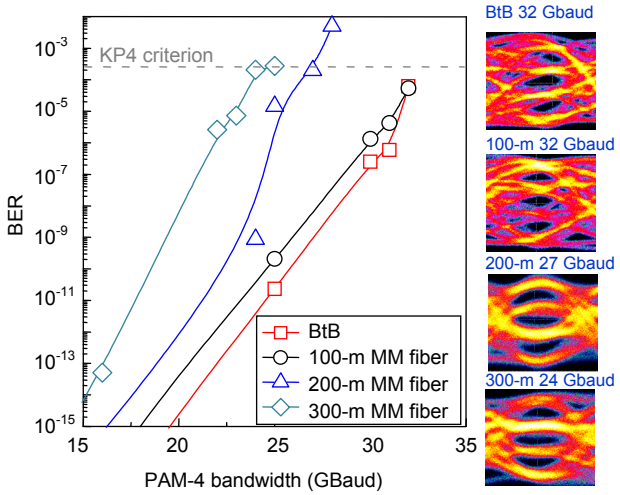

Fig. 9 | BERs of the SM VCSEL chip carried and data waveform pre-emphasized PAM-4 data at different bandwidths after BtB, 100-m, 200-m, and 300-m OM4 MMF transmissions with the corresponding eye-diagram.

To further utilize the bandwidth of laser, the quadrature amplitude modulation orthogonal frequency division multiplexing (QAM-OFDM) was proposed to solve this problem[41-43]. In addition, the Hermitian symmetry is used to obtain a real-valued time-domain signal, which is called as the discrete multitone (DMT) regarded as a special case of OFDM data format to modulate the VCSEL[44,45]. In 2015, Lu et al. even used the discrete multi-tone algorithm (DMT) data format to modulate SM VCSEL with the modulation bandwidth of 12 GHz, which further achieves the data rate to 50 Gbps[46]. In 2016, Puerta et al. used multi-band OFDM data format to demonstrate the ODFM transmission with the data rate of 107.5 Gbps over 10-m MMF[47]. In addition, Tsai et al. employed 850-nm MM VCSEL with the modulation bandwidth of 14 GHz to directly perform the QAM-OFDM transmission in MM fiber[48]. By using the OFDM subcarrier pre-leveling technology to compensate the component of the high-frequency OFDM subcarriers, the signal-to-noise ratio (SNR) above the FEC criterion can be achieved to 13 GHz with the pre-leveling slope of 0.2 dB/GHz over 100-m MM fiber transmission, which makes the 16-QAM-OFDM data transmission obtain the best error vector magnitude (EVM) of 17.1% and the lowest BER of 3.4×10^{-3}.

Moreover, Kao et al. observed the VCSEL with different transverse modes to process the 16-QAM-OFDM data format over 100-m OM4 fiber transmission[49]. The SM VCSEL has the modal-dispersion free characteristic to still be regarded as the best choice for transmitting the versatile data format over 100-m OM4 MM fiber. From Fig. 10, the 100-m MM fiber transmitted 16-QAM-OFDM transmission for SM VCSEL can achieve the data rate of 80 Gbps and the lowest receiving power penalty of 1.8 dB.

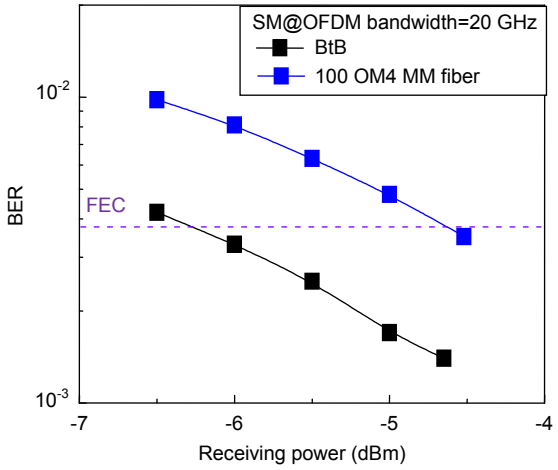

Fig. 10 | BER of the 100-m OM4-MM fiber transmitted 16-QAM-OFDM data for SM VCSEL under the different receiving powers.

Later, the same group utilized the power of the low-frequency OFDM subcarrier to compensate the power of the high-frequency OFDM subcarriers by the pre-leveling technology, which improves the transmission performance of the 100-m OM4 fiber transmitted 16-QAM-OFDM data for the FM VCSEL with the modulation bandwidth of 22 GHz[50]. From Fig. 11(a), the subcarrier BER at a high frequency after 100-m OM4 fiber transmission can be improved by the pre-leveling to further enhance the whole BER. For the 16-QAM OFDM data at 92 Gb/s, the BER response can further be achieved to the FEC criterion at 0.25 dBm by using the pre-leveling technology, as shown in Fig. 11(b).

Other applications

With the great advanced development of information technology in future high-speed internet, the applications and related markets, such as the 5G mobile networks and cloud implementation using smart service systems have become increasingly widespread. Attributed to the expansion of intelligent applications, smart cities/homes can be viewed as a complex, intelligent system that allows all kinds of electronic devices with intelligent monitoring and information transmission capabilities to interact with each other through communication technologies. To build a smart city, the sensing client is one of the most important links in the intelligent service system. For example, the major motor vehicle manufacturers deploy sensors, such as light detection and ranging (LiDAR) and depth-sensing lenses to achieve the goal of fully autono-

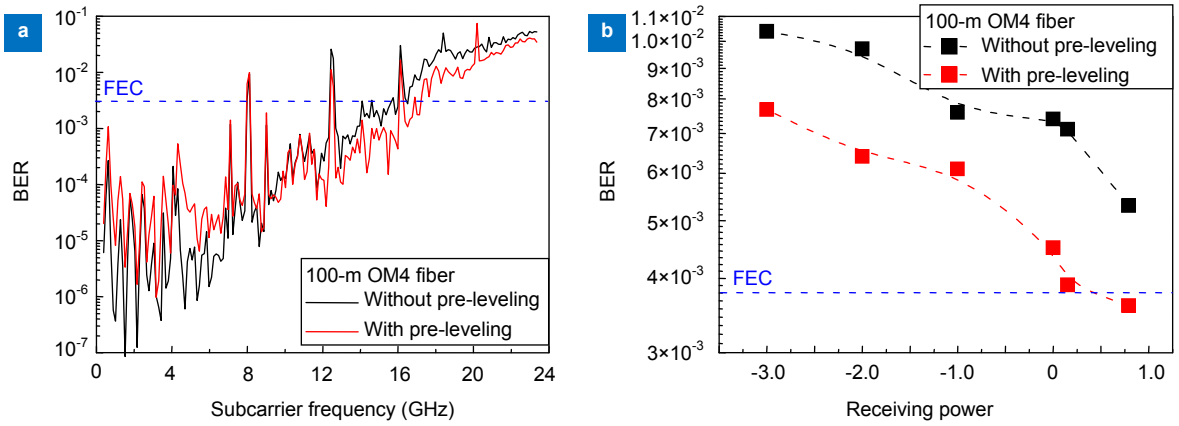

Fig. 11 | (**a**) Subcarrier BER responses of the 16-QAM OFDM data before and after 100-m MMF transmissions. (**b**) BER responses of the FM VCSEL carried 16-QAM OFDM data with and without pre-leveling under 100-m MMF transmissions under different receiving powers.

mous vehicles. LiDAR is an optical telemetry technology. When the optical radar irradiates a laser beam on the target, the distance between the target and the optical radar is measured according to the time of flight of light transmitted and received, and the position information of the target is estimated from the emission and reception angles of the laser light. To date, the direction of laser beam for a sensing system has principally been governed by an external mechanical system that incorporates macroscopic-size optical components including double-swing mirror, galvanometer-driven mirrors and polygon reflecting prism. The traditional sensor–mechanical LiDAR has many disadvantages, e.g., large size, expensive, heavy, high power consumption, low performance, low reliability, and slow scanning speed. The field of view (FOV) of LiDAR is related to beam divergence, the primary beam angle should be in range of 0.1 to 1 milliradian, and small FOV can be used for detailed local mapping, edge detection, and detailed vegetation canopy studies. Large FOV can be used for more complete ground sampling and more interactions with multiple vertical structures.

To achieve the near-infrared laser with the capability of an optical radar component, the laser device must be able to flexibly regulate the emission angle that allows active beam steering. Prof. F. Koyama's group from Tokyo Institute of Technology proposed that the laser beam steering can be successfully achieved by using GaAs-based VCSELs combined with a slow-light Bragg reflector waveguide[51]. Such a hybrid structure is similar to the conventional VCSELs. They demonstrated a continuous beam steering of over 30°, in a good agreement with the simulation results of the deflection angles. The governing mechanism of the angle tuning characteristics is due to the Snell's law. This method uses the refractive index difference between air and semiconductor to deflect the light beam. The deflection angle is strongly dependent on the wavelength.

In 2013, Prof. F. Koyama proposed a high-resolution beam-steering device based on a vertical-cavity surface-emitting laser with a 1-mm-long active-type Bragg reflector waveguide[52]. They showed curved light beams and enormous steering angle by increasing the length of a device. As shown in Fig. 5(b), we can see that parallel radiation beams with constant phase front clearly appeared in the measured far-field patterns. They demonstrated the continuous tuning of the emission angle for incident light consisting of wavelengths from 961 nm to 976 nm and the deflection angle changes over 20°. But this technique needs an antireflection coating at the end of the waveguide and an external light source.

In addition, an optical phased array (OPA) with multiple optical antenna elements may provide equal-intensity coherent signals by modulating the phase of individual antenna. In 2013, J. Sun et al., at Massachusetts Institute of Technology (MIT) demonstrated a large-scale nanophotonic phased array to achieve beam steering built on a silicon photonic platform[53]. The proposed structure consists a 64×64 nanophotonic phased array of nanoantenna, while the array allows direct manipulation of amplitude and phase of emitted light. In the structure, each nanoantenna is in a size of 9 μm×9 μm and connected to a thermal phase tuner which is formed by doped silicon. By applying various electric voltages on each heater in the *X*-*Y* network, dynamic phase modulation can be achieved to generate modulated phase profiles in far-field. This group also proposed the electronically controlled phased array with metallic nanoantennas based on the integrated ohmic thermo-optic phase tuner in the same year[54]. The proposed optical phased array antenna consists of a semiconductor waveguide and a circular aperture antenna. The steering angle of the emitted beam at about 8° was demonstrated by applying the voltage to the individual phase tuner at fixed wavelengths. Simultaneously, a side-lobe separation of about 9° was also clearly observed for linear array with a period of 9 μm (14° for period of 6 μm). The optical phased arrays made by the MIT's group are not easy to be implemented for a small footprint device, because the device could have a lot of nanoantennas to form a high-resolution far-field pattern. The far-field pattern of Fig. 12(a) shows

single transverse mode by well controlled aperture size. The intensity uniformity of the near-field pattern is shown in Fig. 12(b). The temperature of each optical nanoantenna cannot be accurately controlled, and then we should have a concern for the effect of thermal diffusion induced modulational instability.

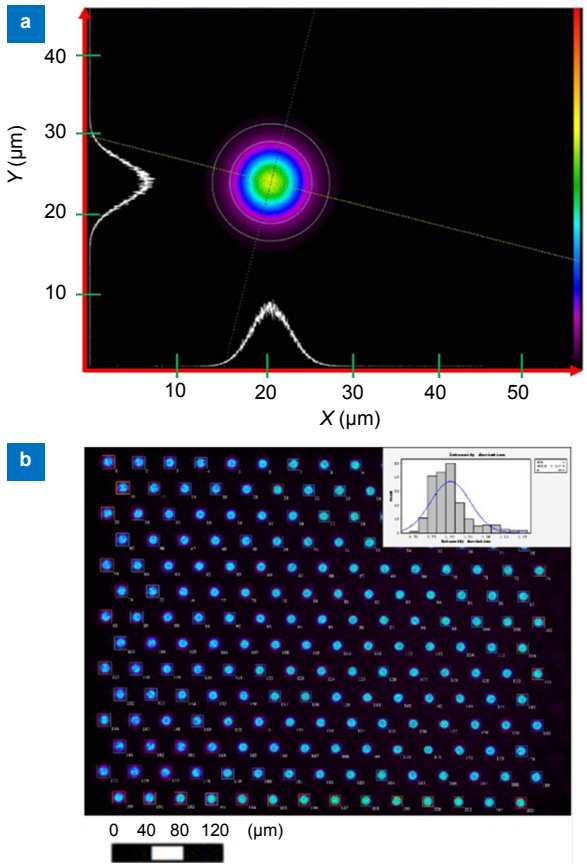

Fig. 12 | (**a**) Far-filed pattern with 6 μm aperture. (**b**) Intensity distribution under 1 A pulse of 2-D arrays.

In 2015, J. C. Hulme, et al. from University of California, Santa Barbara presented the first fully-integrated two-dimensional beam-steering chip on the photonic integrated circuit (PIC) platform[55]. The 2D beam-steering chip can be employed to control the beam propagating directions by actively controlling 164 integrated photonic elements, such as tunable lasers, channel amplifiers, photodiodes, phase tuners, output grating array, and splitters. The working mechanism of the 2D beam-steering device can be introduced as follows. First, the laser light from the light sources with tunable wavelengths is directly launched into the integrated amplifiers. Then, the enhanced light beams are guided to pass through the optical splitters and phase modulators. The split light with different phases are diffracted by the second-order Bragg gratings, forming 2D laser beam scanning profile. The layout of the proposed PIC is within size of 6 mm×11.5 mm. The light emitted from the fully integrated PIC with thermally-controlled phase tuner exhibits that the light deflection angle can be controlled over 23°×3.6° with the beam width of 1°×0.6°.

Conclusions

With the development of VCSEL and application requirements, VCSEL not only played an important role of the high-speed and large-capacity to be applied to the supercomputers, cloud computing, 5G communications, and data centers, also applied to face recognition, light detection and ranging (LiDAR) and VR (virtual reality)/AR (augmented reality)/MR (mixed reality) and so on. Through the increasing diversification of market demand for VCSEL, commercial technology companies and research institutions are following the trend of in-depth research, optimizing VCSEL performance and improving output power. Believed that in the near future, VCSEL will have a better development.

References

1. Westbergh P, Gustavsson J S, Haglund Å, Skold M, Joel A *et al*. High-speed, low-current-density 850 nm VCSELs. *IEEE J Sel Top Quantum Electron* **15**, 694–703 (2009).
2. Healy S B, O'Reilly E P, Gustavsson J S, Westbergh P, Haglund Å *et al*. Active region design for high-speed 850-nm VCSELs. *IEEE J Quantum Electron* **46**, 506–512 (2010).
3. Lear K L, Mar A, Choquette K D, Kilcoyne S P, Schneider Jr R P *et al*. High-frequency modulation of oxide-confined vertical cavity surface emitting lasers. *Electron Lett* **32**, 457–458 (1996).
4. Lear K L, Hietala V M, Hou H Q, Banas J, Hammons B E *et al*. High-speed 850 nm oxide-confined vertical cavity surface emitting lasers. In Nuss M, Bowers J. *Ultrafast Electronics and Optoelectronics* (Optical Society of America, Washington, DC, 1997).
5. Chang Y H, Kuo H C, Lai F I, Tzeng K F, Yu H C *et al*. High speed (>13 GHz) modulation of 850 nm vertical cavity surface emitting lasers (VCSELs) with tapered oxide confined layer. *IEE Proc-Optoelectron* **152**, 170–173 (2005).
6. Ou Y, Gustavsson J S, Westbergh P, Haglund A, Larsson A *et al*. Impedance characteristics and parasitic speed limitations of high-speed 850-nm VCSELs. *IEEE Photon Technol Lett* **21**, 1840–1842 (2009).
7. Liu M, Wang C Y, Feng M, Holonyak N. 50 Gb/s error-free data transmission of 850 nm oxide-confined VCSELs. In *Optical Fiber Communication Conference* 1–3 (Optical Society of America, 2016); http://doi.org/10.1364/OFC.2016.Tu3D.2.
8. Tanigawa T, Onishi T, Nagai S, Ueda T. High-speed 850 nm AlGaAs/GaAs vertical cavity surface emitting laser with low parasitic capacitance fabricated using BCB planarization technique. In *Conference on Lasers and Electro-Optics* 1381–1383 (IEEE, 2005); http://doi.org/10.1109/CLEO.2005.202132.
9. Shi J W, Wei Z R, Chi K L, Jiang J W, Wun J M *et al*. Single-mode, high-speed, and high-power vertical-cavity surface-emitting lasers at 850 nm for short to medium reach (2 km) optical interconnects. *J Lightwave Technol* **31**, 4037–4044 (2013).
10. Mutig A. Physical processes in lasers and VCSEL design. In *High Speed VCSELs for Optical Interconnects* (Springer, Berlin, Heidelberg, 2011: 19–84).
11. Al-Omari A N, Lear K L. VCSELs with a self-aligned contact and

copper-plated heatsink. *IEEE Photon Technol Lett* **17**, 1767–1769 (2005).
12. Larsson A, Westbergh P, Gustavsson J, Haglund Å. High-speed low-current-density 850 nm VCSELs. *Proc SPIE* **7615**, 761505 (2010).
13. Gholami A, Molin D, Sillard P. Compensation of chromatic dispersion by modal dispersion in MMF- and VCSEL-based gigabit Ethernet transmissions. *IEEE Photon Technol Lett* **21**, 645–647 (2009).
14. Blokhin S A, Lott J A, Mutig A, Fiol G, Ledentsov N N *et al*. Oxide-confined 850 nm VCSELs operating at bit rates up to 40 Gbit/s. *Electron Lett* **45**, 501–503 (2009).
15. Westbergh P, Gustavsson J S, Kögel B, Haglund A, Larsson A *et al*. 40 Gbit/s error-free operation of oxide-confined 850 nm VCSEL. *Electron Lett* **46**, 1014–1016 (2010).
16. Szczerba K, Westbergh P, Karout J, Gustavsson J S, Haglund Å *et al*. 4-PAM for high-speed short-range optical communications. *IEEE J Opt Commun Netw* **4**, 885–894 (2012).
17. Choquette K D, Geib K M, Briggs R D, Allerman A A, Hindi J J. Single transverse mode selectively oxidized vertical-cavity lasers. *Proc SPIE* **3946**, 230–233 (2000).
18. Haglund Å, Gustavsson J S, Vukŭsić J, Modh P, Larsson A. Single fundamental-mode output power exceeding 6 mW from VCSELs with a shallow surface relief. *IEEE Photon Technol Lett* **16**, 368–370 (2004).
19. Furukawa A, Hoshi M, Sasaki S, Matsuzono A, Moritoh K *et al*. High-power single-transverse-mode holey VCSELs (Invited Paper). *Proc SPIE* **5722**, 183–190 (2005).
20. Safaisini R, Szczerba K, Westbergh P, Haglund E, Kögel B *et al*. High-speed 850 nm Quasi-single-mode VCSELs for extended-reach optical interconnects. *IEEE J Opt Commun Netw* **5**, 686–695 (2013).
21. Michalzik R, Ebeling K J. Generalized BV diagrams for higher order transverse modes in planar vertical-cavity laser diodes. *IEEE J Quantum Electron* **31**, 1371–1379 (1995).
22. Gustavsson J S, Haglund A, Bengtsson J, Modh P, Larsson A. Dynamic behavior of fundamental-mode stabilized VCSELs using a shallow surface relief. *IEEE J Quantum Electron* **40**, 607–619 (2004).
23. Liu Y, Ng W C, Klein B, Hess K. Effects of the spatial nonuniformity of optical transverse modes on the modulation response of vertical-cavity surface-emitting lasers. *IEEE J Quantum Electron* **39**, 99–108 (2003).
24. Vakhshoori D, Wynn J D, Zydzik G J, Leibenguth R E, Asom M T *et al*. Top‐surface emitting lasers with 1.9 V threshold voltage and the effect of spatial hole burning on their transverse mode operation and efficiencies. *Appl Phys Lett* **62**, 1448–1450 (1993).
25. MacDougal M H, Geske J, Lin C K, Bond A E, Dapkus P D. Low resistance intracavity-contacted oxide-aperture VCSELs. *IEEE Photon Technol Lett* **10**, 9–11 (1998).
26. Harrison I, Ho H P, Tuck B, Henini M, Hughes O H. Zn diffusion-induced disorder in AlAs/GaAs superlattices. *Semicond Sci Technol* **4**, 841–846 (1989).
27. Yang Y J, Dziura T G, Bardin T, Wang S C, Fernandez R. Continuous wave single transverse mode vertical-cavity surface-emitting lasers fabricated by helium implantation and zinc diffusion. *Electron Lett* **28**, 274–276 (1992).
28. Shi J W, Chen C C, Wu Y S, Guol S H, Kuo C *et al*. High-power and high-speed Zn-diffusion single fundamental-mode vertical-cavity surface-emitting lasers at 850-nm wavelength. *IEEE Photon Technol Lett* **20**, 1121–1123 (2008).
29. Kao H Y, Chi Y C, Peng C Y, Leong S F, Chang C K *et al*. Modal linewidth dependent transmission performance of 850-nm VCSELs with encoding PAM-4 over 100-m MMF. *IEEE J Quantum Electron* **53**, 8000408 (2017).
30. Westbergh P, Safaisini R, Haglund E, Kögel B, Gustavsson J S *et al*. High-speed 850 nm VCSELs with 28 GHz modulation bandwidth operating error-free up to 44 Gbit/s. *Elect Lett* **48**, 1145–1147 (2012).
31. Westbergh P, Safaisini R, Haglund E, Gustavsson J S, Larsson A *et al*. High-speed oxide confined 850-nm VCSELs operating error-free at 40 Gb/s up to 85°C. *IEEE Photon Technol Lett* **25**, 768‐771 (2013).
32. Chi K L, Shi Y X, Chen X N, Chen J, Yang Y J *et al*. Single-mode 850-nm VCSELs for 54-Gb/s ON-OFF keying transmission over 1-km multi-mode fiber. *IEEE Photon Technol Lett* **28**, 1367–1370 (2016).
33. Szczerba K, Westbergh P, Agrell E, Karlsson M, Andrekson P A *et al*. Comparison of intersymbol interference power penalties for OOK and 4-PAM in short-range optical links. *J Lightwave Technol* **31**, 3525–3534 (2013).
34. Breyer F, Lee S C J, Randel S, Hanik N. Comparison of OOK- and PAM-4 modulation for 10 Gbit/s transmission over up to 300 m polymer optical fiber. In *Optical Fiber Communication/National Fiber Optic Engineers Conference* 1–3 (IEEE, 2008); http://doi.org/10.1109/OFC.2008.4528669.
35. Ingham J D, Penty R V, White I H, Westbergh P, Gustavsson J S *et al*. 32 Gb/s multilevel modulation of an 850 nm VCSEL for next-generation data communication standards. In *Conference on Lasers and Electro-Optics* 1–2 (IEEE, 2011); http://doi.org/10.1364/CLEO_SI.2011.CWJ2.
36. Szczerba K, Westbergh P, Karlsson M, Andrekson P A, Larsson A. 60 Gbits error-free 4-PAM operation with 850 nm VCSEL. *Elect Lett* **49**, 953–955 (2015).
37. Castro J M, Pimpinella R, Kose B, Huang Y, Lane B *et al*. 200m 2 × 50 Gb/s PAM-4 SWDM transmission over wideband multimode fiber using VCSELs and pre-distortion signaling. In *Optical Fiber Communications Conference and Exhibition* (*OFC*) 1–3 (IEEE, 2016); http://doi.org/10.1364/OFC.2015.W1D.1.
38. Motaghiannezam S M R, Lyubomirsky I, Daghighian H, Kocot C, Gray T *et al*. 180 Gbps PAM4 VCSEL transmission over 300 m wideband OM4 fibre. In *Optical Fiber Communications Conference and Exhibition* (*OFC*) 1–3 (IEEE, 2016); http://doi.org/10.1364/OFC.2016.Th3G.2.
39. Lavrencik J, Varughese S, Thomas V A, Landry G, Sun Y *et al*. 100Gbps PAM-4 transmission over 100m OM4 and wideband fiber using 850nm VCSELs. In *42nd European Conference on Optical Communication* 1–3 (IEEE, 2016).
40. Kao H Y, Tsai C T, Leong S F, Peng C Y, Chi Y C *et al*. Single-mode VCSEL for pre-emphasis PAM-4 transmission up to 64 Gbit/s over 100–300 m in OM4 MMF. *Photon Res*. Accepted 17 Dec 2017. Doc. ID: 312994.
41. Karinou F, Deng L, Lopez R R, Prince K, Jensen J B *et al*. Performance comparison of 850-nm and 1550-nm VCSELs exploiting OOK, OFDM, and 4-PAM over SMF/MMF links for low-cost optical interconnects. *Opt Fiber Technol* **19**, 206–212 (2013).
42. Chi Y C, Li Y C, Wang H Y, Peng P C, Lu H H *et al*. Optical 16-QAM-52-OFDM transmission at 4 Gbit/s by directly modulating a coherently injection-locked colorless laser diode. *Opt Express* **20**, 20071–20077 (2012).
43. Lin C Y, Chi Y C, Tsai C T, Wang H Y, Lin G R. 39-GHz millimeter-wave carrier generation in dual-mode colorless laser diode for OFDM-MMWoF transmission. *IEEE J Sel Top Quantum*

Electron **21**, 1801810 (2015).
44. Lee S C J, Randel S, Breyer F, Koonen A M J. PAM-DMT for intensity-modulated and direct-detection optical communication systems. *IEEE Photon Technol Lett* **21**, 1749–1751 (2009).
45. Barros D J F, Wilson S K, Kahn J M. Comparison of orthogonal frequency-division multiplexing and pulse-amplitude modulation in indoor optical wireless links. *IEEE Trans Commun* **60**, 153–162 (2012).
46. Lu I C, Wei C C, Chen H Y, Chen K Z, Huang C H *et al*. Very high bit-rate distance product using high-power single-mode 850-nm VCSEL with discrete multitone modulation formats through OM4 multimode fiber. *IEEE J Sel Top Quantum Electron* **21**, 1701009 (2015).
47. Puerta R, Agustin M, Chorchos L, Toński J, Kropp J R *et al*. 107.5 Gb/s 850 nm multi- and single-mode VCSEL transmission over 10 and 100 m of multi-mode fiber. In *Optical Fiber Communications Conference and Exhibition* (*OFC*) 1–3 (IEEE, 2016); http://doi.org/10.1364/OFC.2016.Th5B.5.
48. Tsai C T, Peng C Y, Wu C Y, Leong S F, Kao H Y *et al*. Multi-mode VCSEL chip with high-indium-density InGaAs/AlGaAs quantum-well pairs for QAM-OFDM in multi-mode fiber. *IEEE J Quantum Electron* **53**, 2400608 (2017).
49. Kao H Y, Tsai C T, Leong S F, Peng C Y, Chi Y C *et al*. Comparison of single-/few-/multi-mode 850 nm VCSELs for optical OFDM transmission. *Opt Express* **25**, 16347–16363 (2017).
50. Kao H Y, Chi Y C, Tsai C T, Leong S F, Peng C Y *et al*. Few-mode VCSEL chip for 100-Gb/s transmission over 100 m multimode fiber. *Photon Res* **5**, 507–515 (2017).
51. Gu X D, Shimada T, Fuchida A, Matsutani A, Imamura A *et al*. Beam steering in GaInAs/GaAs slow-light Bragg reflector waveguide amplifier. *Appl Phys Lett* **99**, 211107 (2011).
52. Koyama F, Gu X D. Beam steering, beam shaping, and intensity modulation based on VCSEL photonics. *IEEE J Sel Top Quantum Electron* **19**, 1701510 (2013).
53. Sun J, Timurdogan E, Yaacobi A, Hosseini E S, Watts M R. Large-scale nanophotonic phased array. *Nature* **493**, 195–199 (2013).
54. DeRose C T, Kekatpure R D, Trotter D C, Starbuck A, Wendt J R *et al*. Electronically controlled optical beam-steering by an active phased array of metallic nanoantennas. *Opt Express* **21**, 5198–5208 (2013).
55. Hulme J C, Doylend J K, Heck M J R, Peters J D, Davenport M L *et al*. Fully integrated hybrid silicon two dimensional beam scanner. *Opt Express* **23**, 5861–5874 (2015).

Acknowledgements

The authors would like to thank Prof. K Iga and Prof. F Koyama of Tokyo Institute of Technology, Prof. N. Holonyak Jr. and Prof. M. Feng of UIUC, Prof. C. Chang-Hasnain of UC Berkeley, and Prof. S. C. Wang and Prof. T. C. Lu of Chiao Tung University for their insightful suggestions and discussions during the development of GaAs-based VCSEL technology, Crosslight for providing simulation modeling calculate technical support, and Picosun for providing atomic layer deposition technical support. This work was supported by the Ministry of Science and Technology, Taiwan, China (Grants No. MOST 104-2221-E-002-117-MY3, MOST 106-2221- E-002-152-MY3 and MOST 106-2218-E-005-001-) and Excellent Research Projects of Taiwan University (Grant No. NTU-ERP-105R89081).

Competing interests

The authors declare no competing financial interests.